In$_2$O$_3$-Ga$_2$O$_3$ Alloys as Potential Buffer Layers in CdTe Thin-Film Solar Cells

A. Dive [1,2] J. Varley,[2] and S. Banerjee [1,*]

[1] *School of Mechanical and Materials Engineering, Washington State University, Pullman, Washington 99164-2920, USA*
[2] *Lawrence Livermore National Laboratory, Livermore, California 94551-0808, USA*

The efficiency of state-of-the-art CdTe solar cells remains limited by the relatively low open-circuit voltage (V_{OC}). Improving the front interface is key towards realizing a higher V_{OC} after achieving the necessary bulk carrier density and lifetime. Recent efforts in identifying buffer layers beyond CdS have focused on Mg$_x$Zn$_{1-x}$O, which offers tunability of the band offsets, but often suffers from high interfacial defect densities. Ga$_2$O$_3$-based buffer layers demonstrate tremendous improvements in interfacial defect passivation in crystalline silicon and dye-sensitized solar cells, leading to record high V_{OC}, yet remain largely unexplored in CdTe-based devices. Here, we perform hybrid density-functional-theory calculations to investigate pure Ga$_2$O$_3$ and InGaO$_3$ alloys as a window layer in CdTe photovoltaics. We report calculated band offsets for several pairs of solid-solid interfaces comprising transparent conducting oxide (TCO) and CdTe heterojunctions. The results support a large conduction band offset spike of 0.67 eV for the CdTe/Ga$_2$O$_3$ (100) interface, while the offset is reduced to 0.18 eV for the InGaO$_3$ alloy and matches closely with the preferred optimum value of 0.2 eV. Device-level modeling tests of CdTe solar cells integrating our results indicate that the highest efficiency is achieved with InGaO$_3$ acting both as a buffer layer and TCO. Our results suggest that alloys of In$_2$O$_3$ and Ga$_2$O$_3$ may be attractive alternatives to Mg$_x$Zn$_{1-x}$O for tailoring optimal conduction-band offsets of the buffer and TCO layers in high-efficiency CdTe thin-film solar cells.

Thin-film photovoltaic cells based on CdTe [1,2] achieve significantly improved power conversion efficiencies (approximately 20%). Figure 1 presents the typical construction of a CdTe thin-film solar cell. The multilayered structure comprises of a glass substrate; absorber (CdTe); contact or -charge-transport layers, typically involving a buffer layer (e.g., CdS); and an *n*-type transparent conducting oxide (TCO) for electrons and other hole-contact layers (e.g., ZnTe, ZnO).

A representative CdS/CdTe interface band diagram, adopted from Sites and co-workers [3], is presented in Fig. 2(a). The plot shows a negative *cliff-type* conduction-band offset [3] of about 0.1 eV in typical CdTe solar cells with CdS buffer layers. Despite the demonstrated efficiencies of devices with CdS, the electron-hole pairs generated in the CdS emitter layer do not contribute towards the photocurrent due to a significant reduction of the quantum efficiencies for wavelengths <550 nm.[4] This drawback has driven efforts to reduce the thickness of the CdS buffer layer, as well as to find alternative wider-band-gap buffer layers. An optimum conduction-band offset value of +0.2 eV, as shown in Fig. 2(b), represents a small spike

in the conduction band across the emitter and CdTe layers and can lead to high conversion efficiencies [5]. On the other hand, a conduction-band offset >0.4 eV represented in Fig. 2(c) would lead to a lower photocurrent, and thereby, lower the conversion efficiencies.

An emitter material with high transparency and favorable transport properties could also eliminate the need for separate TCO and buffer layers and simplify deposition processes. Recent studies show that tuning the Mg content in Mg$_x$Zn$_{1-x}$O alloys [6–9] can lead to a wider band gap and yield a positive conduction-band offset with the absorber, making it a favorable system for the TCO and emitter layers. Despite these advantages, Mg$_x$Zn$_{1-x}$O has challenges associated with defective interface, chemical stability, and doping; however, its emergence suggests TCO alloys as attractive alternatives to CdS. The efficiency of CdTe solar cells is also limited by a low V_{OC}. Improving the front TCO-absorber interface is key to realizing a higher V_{OC} along with achieving the required bulk carrier density and lifetime. Additionally, suitable passivation of the front and back interface, emitter doping, and improved absorber properties can lead to a CdTe efficiency of up to 28% [10,11].

The objective of this research effort is to study Ga$_2$O$_3$ and its alloys with In$_2$O$_3$ as a potential heterojunction
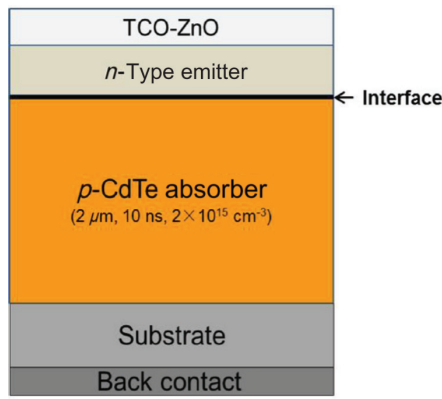
FIG. 1. Representative CdTe thin-film structure is shown. Reproduced from Ref. [3] with the permission of AIP Publishing.

partner for CdTe solar cells. Ga_2O_3-based TCO layers demonstrate tremendous improvements in interfacial defect passivation in crystalline silicon and dye-sensitized solar cells, leading to a record high V_{OC} [12–16]. Ga_2O_3 exhibits promising electro-optical properties that can potentially improve the conversion efficiencies for CdTe solar cells. For instance, Ga_2O_3 exhibits transparency to wavelengths of about 250 nm [17–20]. Easy fabrication of both bulk crystals and thin films, along with wider control over the electrical properties from semi-insulating to degenerate doping, are some of the promising features that can be leveraged in CdTe thin-film photovoltaic technologies.

Several studies report that the theoretical band gap for Ga_2O_3 is about 4.6–4.9 eV [21–23]. However, conduction-band offsets across the CdTe/Ga_2O_3 interface have not been thoroughly investigated. Here, we evaluate these

conduction-band offsets using calculations based on hybrid density-functional theory (DFT). A large band gap for Ga_2O_3 could possibly lead to the large spike type feature shown in Fig. 2(c). Tuning of the large band gap of Ga_2O_3 can be achieved through appropriate doping and alloying. Doping Ga_2O_3 with various elements is reported to lower the band gap [24–28], with In incorporation predicted to both lower the band gap and tune the electron affinity [29–35]. Pure In_2O_3 has a relatively low band gap of about 2.6–2.9 eV [36], which can lower the band offset. The transparency limitations associated with In_2O_3 [37] restrict its use as TCO material for CdTe thin-film photovoltaics. Additionally, Rüggeberg and Klein [38] have studied the In_2O_3/CdTe interface through reactive evaporation of In. They report a negligible (~0 eV) conduction-band offset across the In_2O_3/CdTe interface. However, they claim that, despite an aligned conduction-band offset, In_2O_3 as a TCO is still detrimental to the CdTe solar cell, owing to the Fermi-level positioning for In_2O_3/CdTe (0.6 eV below the CdTe conduction-band maximum). As a result, pure In_2O_3 is not a favorable candidate as a TCO material for CdTe thin-film photovoltaics. In_2O_3 alloying with Ga_2O_3 would offer a sufficiently wide range (~2.6–4.8 eV) of band gaps for $In_xGa_{2-x}O_3$ alloys coupled with the superior transparency properties [39,40] of Ga_2O_3. The $In_xGa_{2-x}O_3$ alloys can possibly achieve a conduction-band offset of about +0.2 eV, corresponding to a small spike, which can improve the performance of CdTe solar cells. Boudour *et al.* [41] reported the use of Ga-doped $Mg_xZn_{1-x}O$ materials as a potential TCO and a buffer for high-performance CdTe solar cells. They too have considered a conduction-band offset value of about +0.21 eV across the Ga-doped $Mg_xZn_{1-x}O$/CdTe interface. Additionally, Ga_2O_3 and its alloys can be grown
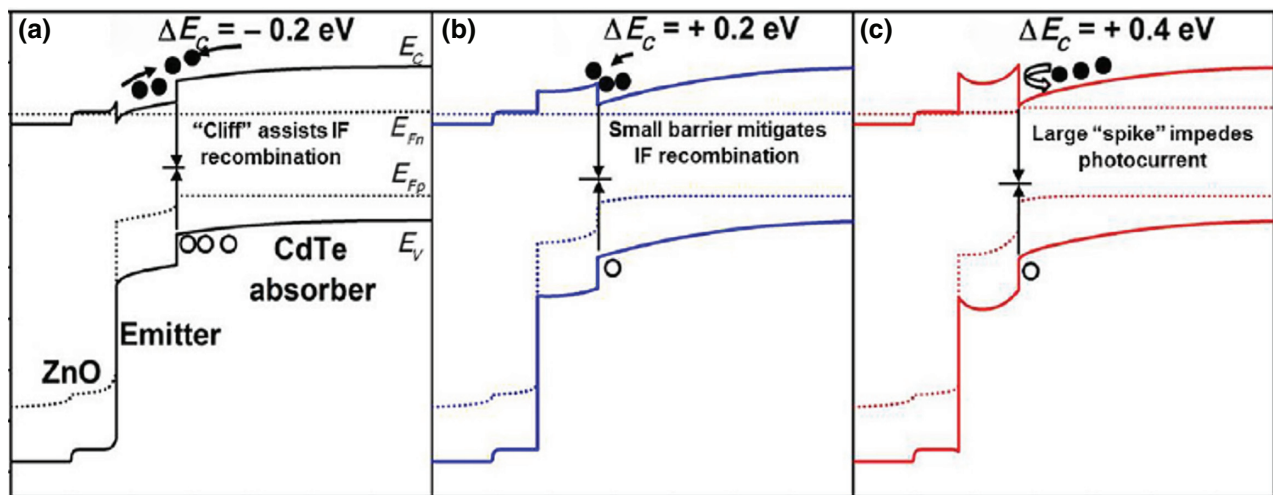

FIG. 2. Representative conduction-band offsets for (a) CdS/CdTe interface showing a "cliff" feature. Optimal recommended emitter and CdTe conduction-band offset values for (b) "spike" and (c) "large spike" features. Reproduced from Ref. [3] with the permission of AIP Publishing. IF, Interface.

using both bulk crystal methods and industrially implementable thin-film deposition methods, such as molecular beam epitaxy [42,43], atomic layer deposition [44,45], magnetron sputtering [46,47], and hydrothermal synthesis [48,49], which can possibly reduce the fabrication costs. Therefore, Ga$_2$O$_3$ and In$_x$Ga$_{2-x}$O$_3$ alloys present attractive analogues to Mg$_x$Zn$_{1-x}$O for incorporation in CdTe photovoltaics. Here, we report the computed band offsets for semiconductor interfaces comprising CdTe and In$_x$Ga$_{2-x}$O$_3$ ($0 < x < 1$) compositions using a hybrid DFT approach [50–53]. To evaluate the impact of the band offset on the conversion efficiencies and V_{OC}, we perform numerical modeling of CdTe solar cells, with Ga$_2$O$_3$ and InGaO$_3$ as the TCO. The band offsets for Ga$_2$O$_3$/CdTe and InGaO$_3$ (50:50 alloy)/CdTe interfaces obtained from DFT calculations coupled with numerical modeling data provide valuable guidance towards the experimental design of preferable In$_x$Ga$_{2-x}$O$_3$-based TCO compositions that can enable high conversion efficiencies in CdTe solar cells.

We perform DFT calculations by employing the QUICK-STEP [54] algorithm of the CP2K [55] package, employing the Gaussian and plane waves (GPW) approach. We utilize Goedecker-Teter-Hutter (GTH) type basis sets, optimized for molecular calculations (MOLOPT) [56], along with GTH pseudopotentials [57] for DFT calculations. Additional details of the DFT calculations are provided in the Supplemental Material (Table S1) [58].

To accurately predict these properties for Ga$_2$O$_3$, InGaO$_3$, and CdTe, we employ the PBE0 [59] hybrid functional, along with the auxiliary density matrix method (ADMM) [60]. The Hartree-Fock mixing ratios selected are 30% for Ga$_2$O$_3$ and GaInO$_3$ and 20% for CdTe, to match the experimental band gaps. The interface supercells shown in Fig. 3 are created using the Interface Builder tool [61,62] as a part of the QuantumATK [63] package. Mu *et al.* [64] have reported the [100]-*B* surface to be the
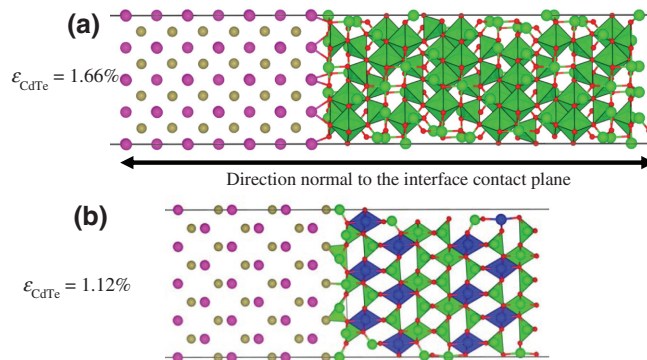

FIG. 3. (a) Ga$_2$O$_3$/CdTe and (b) InGaO$_3$/CdTe interface structures are shown. Green, red, blue, magenta, and brown spheres represent Ga, O, In, Cd, and Te atoms, respectively. In atoms in InGaO$_3$ in (b) only occupy the octahedral sites in the β-gallia structure. Effective strain on CdTe unit cell is reported.

TABLE I. Details of different CdTe cells considered for cell-level modeling.

Cell Name	Absorber layer	Buffer layer	TCO layer
SC1	*p*-CdTe	*n*-CdS	SnO$_x$
SC2	*p*-CdTe	*n*-Ga$_2$O$_3$ (high doping)	SnO$_x$
SC3	*p*-CdTe	*n*-Ga$_2$O$_3$ (high doping)	UID-Ga$_2$O$_3$
SC4	*p*-CdTe	*n*-InGaO$_3$ (high doping)	SnO$_x$
SC5	*p*-CdTe	*n*-InGaO$_3$ (high doping)	UID-InGaO$_3$
SC6	*p*-CdTe	*n*-InGaO$_3$ (high doping)	

most stable for β-Ga$_2$O$_3$. Therefore, we consider the [100] surfaces for β-Ga$_2$O$_3$, InGaO$_3$, and CdTe to form the interface. The details related to the generation of the interface supercells are provided in the Supplemental Material [58]. Van de Walle and co-workers devised a suitable route that accurately calculated the respective electronic properties at relatively low computational costs [65]. We utilize an identical approach to evaluate the band offsets for Ga$_2$O$_3$/CdTe and InGaO$_3$/CdTe interfaces, wherein the band-alignment calculations are performed using PW DFT methods. Additional details are provided in the Supplemental Material [58].

Numerical modeling of photovoltaic CdTe solar cells is performed using the SCAPS software package [66]. Based on the CdTe thin-film architecture shown in Fig. 1, we generate a total of five different photovoltaic CdTe cells with Ga$_2$O$_3$ and InGaO$_3$ as different constituent layers in the cell. UID refers to unintentionally doped layers. Table I provides the details of each of cell with different layer compositions that are considered for cell-level modeling.

Details of the different model constructions and the layer properties are provided in the Supplemental Material [58]. These device models give some insight into the use of dopant grading in the TCO and buffer layers to favorably control carrier transport and charge extraction.

The optimized lattice parameters (provided in Table S2 within the Supplemental Material [58]) for bulk β-Ga$_2$O$_3$, InGaO$_3$, and CdTe show a good match (within 5%) for the reported values from experiments and previous theoretical calculations. The InGaO$_3$ (50:50 alloy) relaxed structure maintains the β-monoclinic structure, in accordance with prior reports [31,32]. The direct electronic band gap at the Γ point calculated with PBE0 are reported in the Supplemental Material (Table S3) [58]. Indium alloying lowers the band gap of Ga$_2$O$_3$ to 4.04 eV from 4.84 eV. The lowering of the band gap with the incorporation of In into Ga$_2$O$_3$ [29] provides an analogous, but opposite, effect to that of Mg incorporation in Mg$_x$Zn$_{1-x}$O. Similar to Mg$_x$Zn$_{1-x}$O, the alloy composition also influences the overall band-edge positions. Owing to the common oxygen-derived character of the valence-band maxima in Ga$_2$O$_3$ and InGaO$_3$, a stronger effect on the conduction-band position may be expected upon In incorporation [30,67]. In the following
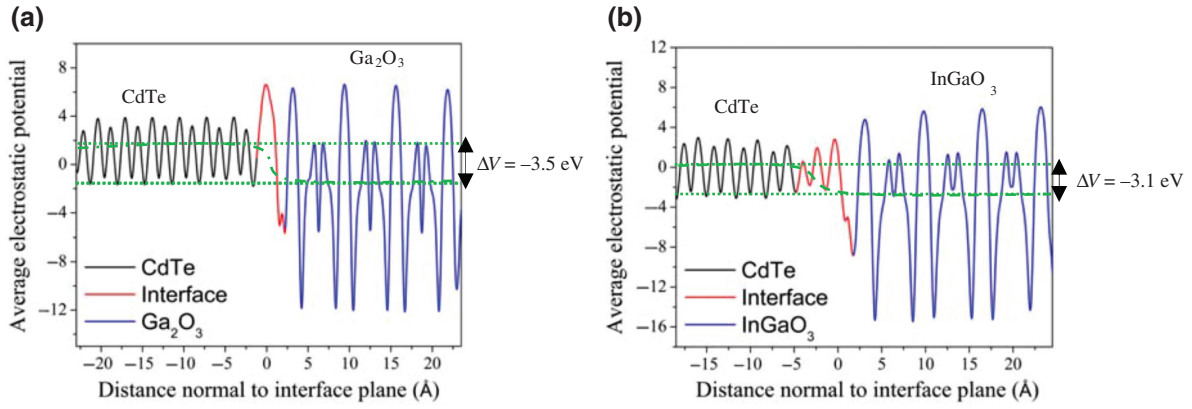
FIG. 4. Average electrostatic potential variations along the direction normal to the interface plane for (a) CdTe/Ga_2O_3 and (b) CdTe/$InGaO_3$. Green line shows a macroscopic average, which reaches a constant value within the bulk CdTe, Ga_2O_3, and $InGaO_3$ regions along the interface.

sections, we will evaluate the impact of changes to the band gap on the band offsets across the CdTe/Ga_2O_3 and CdTe/$InGaO_3$ interfaces.

We calculate the band alignments across the CdTe/Ga_2O_3 and CdTe/$InGaO_3$ interfaces from the planar average electrostatic potential plots shown in Figs. 4(a) and 4(b), respectively. The bulk band alignment (ΔV) is defined as the difference between these constant average electrostatic potentials of the bulk materials forming an interface.

Figure 5 shows the representative band diagram for (a) CdTe/Ga_2O_3 and (b) CdTe/$InGaO_3$ interfaces along the [100] surfaces. The valence-band maximum (VBM) is typically referenced with respect to the bulk average electrostatic potential, as shown in the band diagrams. The negative band-alignment value corresponds a relatively higher positioning of the valence band of CdTe with respect to that of Ga_2O_3 and $InGaO_3$. Based on the band diagrams, we calculate the conduction-band and the valence-band offsets using the following equations [65], which are summarized in Table II:

$$\Delta E_V = [E_{VBM} \, (\text{CdTe}) - E_{VBM} \, (\text{Ga}_2\text{O}_3/\text{InGaO}_3)] - \Delta V, \tag{1}$$

$$\Delta E_C = E_{gap} \, (\text{Ga}_2\text{O}_3/\text{InGaO}_3) - E_{gap} \, (\text{CdTe}) - \Delta E_V. \tag{2}$$

The results show a large conduction-band offset, representative of a sharp spike in the conduction-band offset, for the CdTe/Ga_2O_3 interface. Such a high value of conduction-band offset is detrimental to the efficiency of the CdTe photovoltaic cells. A very high intrinsic band gap for pure β-Ga_2O_3 leads to such a high conduction-band offset for Ga_2O_3/CdTe interfaces. As a result, pure β-Ga_2O_3 is not likely to be an ideal choice for the TCO to achieve a high conversion efficiency in CdTe photovoltaics.

The conduction-band offset for the $InGaO_3$/CdTe interface is +0.18 eV, indicating a small spike for the $InGaO_3$ conduction band relative to that of CdTe. This is 0.49 eV lower than that calculated for the CdTe/Ga_2O_3 conduction-band offset summarized in Table II. The band gap for strained CdTe does not show any significant change for CdTe/Ga_2O_3 and CdTe/$InGaO_3$ interfaces, since the respective strains on CdTe in both interface structures are
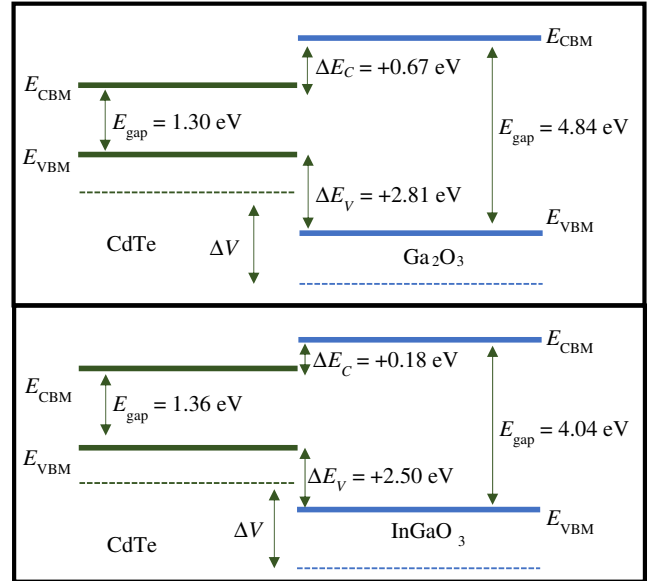

FIG. 5. Representative band structures of (a) CdTe/Ga_2O_3 and (b) CdTe/$InGaO_3$ interfaces, showing conduction- and valence-band offsets. Dashed lines represent the average electrostatic potential for bulk Ga_2O_3, $InGaO_3$, and CdTe. E_{VBM} and E_{CBM} represent valence-band maxima and conduction-band minima, respectively, for Ga_2O_3, $InGaO_3$, and CdTe. ΔE_C and ΔE_V represent conduction- and valence-band offsets, respectively. ΔV is the band alignment, as calculated earlier.

TABLE II. Band offset calculations for CdTe/Ga$_2$O$_3$ and CdTe/InGaO$_3$ interfaces with strained CdTe layers.

	VBM (eV)	E_{gap} (eV)	Band alignment Δ(V-V_{CdTe}) (eV)	ΔE_V (eV)[a]	ΔE_C (eV)[a]
Strained CdTe	1.76	1.30	−3.5	+2.81	+0.67
Ga$_2$O$_3$	2.45	4.84			
Strained CdTe	1.82	1.36	−3.1	+2.5	+0.18
InGaO$_3$	2.42	4.04			

[a]Valence-band (ΔE_V) and conduction-band (ΔE_C) offset values are reported relative to the CdTe band edges.

very similar, as reported in Fig. 3. The valence-band offset shows a very small decrease for the InGaO$_3$/CdTe interface with respect to the valence-band offset for Ga$_2$O$_3$/CdTe interface. Hence, this reported decrease in the conduction-band offset can only be attributed to lowering of the band gap for InGaO$_3$ (4.04 eV), compared with that of Ga$_2$O$_3$ (4.84 eV). In alloying in Ga$_2$O$_3$ shows conduction-band bending behavior, as reported earlier. This conduction-band bending results in significant lowering of the conduction-band energy level for InGaO$_3$, leading to decrease in the band gap. The calculated conduction-band offset of +0.18 eV for InGaO$_3$/CdTe matches closely with the optimum value corresponding to a spike feature shown in Fig. 2(b). Therefore, the theoretical band-offset calculations show that the TCO employing In-doped Ga$_2$O$_3$ has remarkable potential to be used in CdTe thin-film solar cells. To determine the realistic impacts of these properties, we calculate the performance of cells employing these TCO layers, as discussed below.

Table III compares the characteristic properties of different cell models, as mentioned earlier in methodology obtained from numerical modeling studies with the SCAPS software package.

The numerical modeling results show poor performance for cell models SC2 and SC3, compared with the base-level model SC1. For the SC2 and SC3 models, with n-Ga$_2$O$_3$ as a buffer layer along with UID-Ga$_2$O$_3$ as a

TABLE III. Characteristics properties for different cell architectures, as calculated from SCAPS software.

Cell model name	V_{OC} (meV)	J_{SC} (mA/cm^2)	FF (%)	$\eta_{conversion}$ (%)
SC1 (base level)	859.8	24.1161	77.82	16.14
SC2[a]	490.2	24.9802	51.58	6.32
SC3	—	—	—	—
SC4	858.4	25.2428	78.49	17.01
SC5	859.2	26.0758	78.48	17.59
SC6	859.4	26.0759	78.45	17.58

[a]Performance reported for SC2 can only be achieved with an unreasonably high dopant concentration of 9.0×10^{21}/cm^3.

TCO layer, there is no measurable performance obtained from the numerical model, despite considering a very high dopant concentration ($\sim 1 \times 10^{19}$/cm^3) in the n-Ga$_2$O$_3$ buffer layer. The previously calculated conduction-band-offset value for CdTe/Ga$_2$O$_3$ represents a sharp spike feature (arising from +0.67 eV), which is detrimental to the performance of the CdTe solar cell. The numerical modeling results reported in Table III align with the above hypothesis. The decrease in the conversion efficiency, as well as other characteristic properties, is directly correlated to such a high conduction-band offset (+0.67 eV) across the CdTe/Ga$_2$O$_3$ interface.

With In alloying, the conduction-band-offset value can be lowered to a more favorable value of +0.18 eV for the CdTe/InGaO$_3$ interface. Table III shows a significant improvement in the efficiency and open-circuit voltage when n-InGaO$_3$ is used as a buffer layer (SC4–SC6). The conduction-band offset decreases by about 0.49 eV for the 50:50 alloy, compared with that of pure β-Ga$_2$O$_3$. Swallow et al. [68–82] evaluated the conduction-band-offset values for (In$_x$Ga$_{1-x}$)$_2$O$_3$ alloys with common cation semiconductors. They report a conduction-band offset of about 0.45 eV between β-Ga$_2$O$_3$ and InGaO$_3$. This value matches very closely with the difference in the conduction-band offset for β-Ga$_2$O$_3$ and InGaO$_3$ in the present study, thereby providing suitable experimental validation. As mentioned earlier, Rüggeberg and Klein [38] reported aligned conduction bands for In$_2$O$_3$/CdTe. However, they considered the optical band gap of In$_2$O$_3$ to be 3.6 eV, which is significantly higher than the corrected optical band gap of 2.9 eV for In$_2$O$_3$. This corrected value of the optical band gap would reduce the conduction-band offset from about 0 eV to about −0.7 eV for In$_2$O$_3$/CdTe. Such a conduction-band offset would represent a sharp cliff-type conduction-band offset and would lead to increased interface recombination. As a result, the performance of the CdTe solar cell would deteriorate, as reported by Rüggeberg and Klein. Our calculations thereby provide a quantitative trend in decrease of the conduction-band offset with In alloying for the Ga$_2$O$_3$/CdTe interface.

The highest conversion efficiency is observed for the SC5 cell, where n-InGaO$_3$ is used a buffer layer and an additional UID-InGaO$_3$ layer with intrinsic n-type doping as a TCO layer. Moderately doped n-InGaO$_3$ can

also be utilized as a buffer layer and TCO, which shows an increase in the V_{OC} value with a sufficiently high conversion efficiency. Overall, the numerical results indicate that In_2O_3 alloying with Ga_2O_3 can suitably tune the high band gap for β-Ga_2O_3, making $In_xGa_{2-x}O_3$ a promising candidate for replacing the CdS buffer layer and TCO in conventional CdTe solar cells. Further experimental studies to evaluate the quality of interfaces will be necessary to assess the viability of $In_xGa_{2-x}O_3$ as alternatives to $Mg_xZn_{1-x}O$ in state-of-the-art CdTe-based devices.

The conduction-band offset at the TCO/absorber (CdTe) interface plays a crucial role in determining the performance of the CdTe solar cells. A small spike, corresponding to a conduction-band offset of about $+0.2$ eV, is preferred to ensure low carrier recombination across the TCO/CdTe interface and improve the overall efficiencies of the CdTe solar cells. In the present study, we explore Ga_2O_3 and $In_xGa_{2-x}O_3$ alloys as a potential TCO in CdTe solar cells. We employ DFT methods to calculate the band offsets across Ga_2O_3/CdTe and $InGaO_3$/CdTe interfaces. The interfaces are formed with [100] surfaces for Ga_2O_3, $InGaO_3$, and CdTe. The calculated conduction-band offset across the Ga_2O_3/CdTe interface is $+0.67$ eV. The large value of $+0.67$ eV can be attributed to a significantly wider band gap (4.84 eV) for Ga_2O_3. A large conduction-band offset would inhibit the transport of charge carriers across the TCO/CdTe interface and lead to a decrease in conversion efficiencies for CdTe solar cells. Alloying with In_2O_3 to the form $InGaO_3$ (50:50, In:Ga) alloy lowers the band gap to 4.04 eV. The decrease in the band gap is predominantly caused by a lowering of the conduction band and a nominal increase in the valence band. As a result, the conduction-band offset across the $InGaO_3$/CdTe interface decreases significantly to a value of $+0.18$ eV. The theoretical conduction-band offset for $InGaO_3$[100]/CdTe[100] matches closely to the preferred optimum value of $+0.2$ eV. Hence, In_2O_3 alloying with Ga_2O_3 can effectively lower the conduction-band offset to a preferred optimum value, making them potential TCO materials for CdTe solar cells. Lowering the conduction-band offset can significantly improve the conversion efficiencies of the CdTe solar cells, as predicted by our full-cell calculations with SCAPS software. Within our model structures, the maximum theoretical conversion efficiency of 17.59% is achieved for a device employing an n-$InGaO_3$ buffer layer with a UID-$InGaO_3$ TCO construction. In_2O_3 alloying shows the high tunability of the band gap with an In content that can yield a favorable conduction-band offset across the absorber-buffer interfaces. High doping capabilities and a relatively high band gap of In-alloyed Ga_2O_3 makes $In_xGa_{2-x}O_3$ an exciting prospect as both the TCO and buffer layer in CdTe solar cells.

[1] Y. Zhao, M. Boccard, S. Liu, J. Becker, X. H. Zhao, C. M. Campbell, E. Suarez, M. B. Lassis, Z. Holman, and Y.-H. Zhang, Monocrystalline CdTe solar cells with open-circuit voltage over 1 V and efficiency of 17%, Nat. Energy **1**, 16067 (2016).

[2] J. Sites, A. Munshi, J. Kephart, D. Swanson, and W. S. Sampath, in *43rd IEEE Photovolt. Spec. Conf.* (2016), pp. 3632.

[3] T. Song, A. Kanevce, and J. Sites, Emitter/absorber interface of CdTe solar cells, J. Appl. Phys. **119**, 233104 (2016).

[4] Andreas Klein, Energy band alignment in chalcogenide thin film solar cells from photoelectron spectroscopy, J. Phys. Condens. Matter **27**, 134201 (2015).

[5] B. E. McCandless and J. R. Sites, in *Handbook of Photovoltaic Science and Engineering*, edited by A. Luque, S. Hegedus (John Wiley, Chichester, 2013), Vol. 617.

[6] M. Gloeckler and J. R. Sites, Efficiency limitations for wide-band-gap chalcopyrite solar cells, Thin Solid Films **480**, 241 (2005).

[7] J. M. Kephart, J. W. McCamy, Z. Ma, A. Ganjoo, F. M. Alamgir, and W. S. Sampath, Band alignment of front contact layers for high-efficiency CdTe solar cells, Sol. Energy Mater. Sol. Cells **157**, 266 (2016).

[8] T. Minemoto, Y. Hashimoto, T. Satoh, T. Negami, H. Takakura, and Y. Hamakawa, $Cu(In, Ga)Se_2$ solar cells with controlled conduction band offset of window/$Cu(In, Ga)Se_2$ layers, J. Appl. Phys. **89**, 8327 (2001).

[9] T. Torndahl, C. Platzer-Bjorkman, J. Kessler, and M. Edoff, Atomic layer deposition of $Zn_{1-x}Mg_xO$ buffer layers for $Cu(In, Ga)Se_2$ solar cells, Prog. Photovoltaics: Res. Appl. **15**, 225 (2007).

[10] J. N. Duenow and W. K. Metzger, Back-surface recombination, electron reflectors, and paths to 28% efficiency for thin-film photovoltaics: A CdTe case study, J. Appl. Phys. **125**, 053101 (2019).

[11] T. Ablekim, E. Colegrove, and W. K. Metzger, Interface engineering for 25% CdTe solar cells, Appl. Energy Mater. **1**, 5135 (2018).

[12] T. Allen and A. Cuevas, Plasma enhanced atomic layer deposition of gallium oxide on crystalline silicon: Demonstration of surface passivation and negative interfacial charge, Phys. Status Solidi RRL **9**, 220 (2015).

[13] D. Chua, S. Bok Kim, and R. Gordon, Enhancement of the open circuit voltage of Cu_2O/Ga_2O_3 heterojunction solar cells through mitigation of interfacial recombination, AIP Adv. **9**, 55203 (2019).

[14] Y. S. Lee, D. Chua, R. Brandt, S. C. Siah, J. V. Li, J. Mailoa, S. W. Lee, R. Gordon, and T. Buonassisi, Atomic layer

deposited gallium oxide buffer layer enables 1.2 V open-circuit voltage in cuprous oxide solar cells, Adv. Mater. **26,** 4704 (2014).

[15] A. Chandiran, M. Nazeeruddin, and M. Gratzel, The role of insulating oxides in blocking the charge carrier recombination in Dye-sensitized solar cells, Adv. Funct. Mater. **24,** 1615 (2014).

[16] A. Chandiran, N. Tetreault, R. Humphry-Baker, F. Kesseler, E. Baranoff, C. Yi, M. Nazeeruddin, and M. Gratzel, Sub-nanometer Ga$_2$O$_3$ tunneling layer by atomic layer deposition to achieve 1.1 V open-circuit potential in dye-sensitized solar cells, Nano Lett. **12,** 3941 (2012).

[17] T. Onuma, S. Saito, K. Sasaki, T. Masui, T. Yamaguchi, T. Honda, and M. Higashiwaki, Valence band ordering in β-Ga$_2$O$_3$ studied by polarized transmittance and reflectance spectroscopy, Jpn. J. Appl. Phys. **54,** 112601 (2015).

[18] K. Akaiwa and S. Fujita, Electrically conductive corundum-structured α-Ga$_2$O$_3$ thin films on sapphire with tin-doping grown by spray assisted mist chemical vapor deposition, Jpn. J. Appl. Phys. **51,** 070203 (2012).

[19] S. Fujita, M. Oda, K. Kaneko, and T. Hitora, Evolution of corundum-structured III-oxide semiconductors: Growth, properties, and devices, Jpn. J. Appl. Phys. **55,** 1202A3 (2016).

[20] H. H. Tippins, Optical absorption and photoconductivity in the band edge of β-Ga$_2$O$_3$, Phys Rev **140,** 316 (1965).

[21] H. He, M. A. Blanco, and R. Pandey, Electronic and thermodynamic properties of β-Ga$_2$O$_3$, Appl. Phys. Lett. **88,** 261904 (2006).

[22] C. Janowitz, V. Scherer, M. Mohamed, A. Krapf, H. Dwelk, R. Manzke, Z. Galazka, R. Uecker, K. Irmscher, and R. Fornari, Experimental electronic structure of In$_2$O$_3$ and Ga$_2$O$_3$, New J. Phys. **13,** 085014 (2011).

[23] M. J. Tadjerz, J. L. Lyons, N. Nepal, J. A. Freitas Jr, A. D. Koehler, and G. M. Foster, Theory and characterization of doping and defects in β-Ga$_2$O$_3$, J. Solid State Sci. Technol. **8,** Q3187 (2019).

[24] E. Ahmadi, O. S. Koksaldi, S. W. Kaun, Y. Oshima, D. B. Short, U. K. Mishra, and J. S. Speck, Ge doping of β-Ga$_2$O$_3$ films grown by plasma-assisted molecular beam epitaxy, Appl. Phys. Express **10,** 041102 (2017).

[25] A. Kuramata, K. Koshi, S. Watanabe, Y. Yamaoka, T. Masui, and S. Yamakoshi, High-quality β-Ga$_2$O$_3$ single crystals grown by edge-defined film-fed growth, Jpn. J. Appl. Phys. **55,** 1202A2 (2016).

[26] E. G. Villora, K. Shimamura, Y. Yoshikawa, T. Ujiie, and K. Aoki, Electrical conductivity and carrier concentration control in β-Ga$_2$O$_3$ by Si doping, Appl. Phys. Lett. **92,** 20212 (2008).

[27] W. Zhou, C. Xia, Q. Sai, and H. Zhang, Controlling n-type conductivity of β-Ga$_2$O$_3$ by Nb doping, Appl. Phys. Lett. **111,** 242103 (2017).

[28] H. Cui, H. F. Mohamed, C. Xia, Q. Sai, W. Zhou, H. Qi, J. Zhao, J. Si, and X. Ji, Tuning electrical conductivity of β-Ga$_2$O$_3$ single crystals by Ta doping, J. Alloys Compd. **788,** 925 (2019).

[29] H. von Wenckstern, Group-III sesquioxides: Growth, physical properties and devices, Adv. Electron. Mater. **3,** 1600350 (2017).

[30] H. Peelaers, D. Steiauf, J. B. Varley, A. Janotti, and C. G. Van de Walle, (In$_x$ga$_{1-x}$)$_2$O$_3$ alloys for transparent electronics, Phys. Rev. B **92,** 085206 (2015).

[31] R. D. Shannon and C. T. Prewitt, Synthesis and structure of phases in the In$_2$O$_3$-Ga$_2$O$_3$ system, J. Inorg. Nucl. Chem. **30,** 1389 (1968).

[32] D. D. Edwards, P. E. Folkins, and T. O. Mason, Phase equilibria in the Ga$_2$O$_3$-In$_2$O$_3$ system, J. Am. Ceram. Soc. **80,** 253 (1997).

[33] A. Kudo and I. Mikami, Photocatalytic activities and photophysical properties of Ga$_{2-x}$In$_x$O$_3$ solid solution, J. Chem. Soc., Faraday Trans. **94,** 2929 (1998).

[34] T. Oshima and S. Fujita, Properties of Ga$_2$O$_3$-based (In$_x$Ga$_{1-x}$)$_2$O$_3$ alloy thin films grown by molecular beam epitaxy, Phys. Status Solidi C **5,** 3113 (2008).

[35] V. I. Vasyltsiv, Y. I. Rym, and Y. M. Zakharko, Optical absorption and photoconductivity at the band edge of β-Ga$_{2-x}$In$_x$O$_3$, Phys. Status Solidi B **195,** 653 (1996).

[36] K. Irmscher, M. Naumann, M. Pietsch, Z. Galazka, R. Uecker, T. Schulz, R. Schewski, M. Albrecht, and R. Fronari, On the nature and temperature dependence of the fundamental band gap of In$_2$O$_3$, Phys. Status Solidi A **211,** 54 (2014).

[37] H. Peelaers, E. Kioupakis, and C. G. Van de Walle, Limitations of In$_2$O$_3$ as a transparent conducting oxide, Appl. Phys. Lett. **115,** 082105 (2019).

[38] F. Rüggeberg and A. Klein, The In$_2$O$_3$/CdTe interface: A possible contact for thin film solar cells?, Appl. Phys. A **82,** 281 (2016).

[39] W. L. Huang, M. H. Hsu, S. P. Chang, S. J. Chang, and Y. Z. Chiou, Indium gallium oxide thin film transistor for Two-stage UV sensor application, ECS J. Solid State Sci. Technol. **8,** Q3140 (2019).

[40] J. Sheng, E. J. Park, B. Shong, and J. S. Park, Atomic layer deposition of an indium gallium oxide thin film for thin-film transistor applications, ACS Appl. Mater. Interfaces **9,** 23934 (2017).

[41] S. Boudour, I. Bouchama, N. Bouarissa, and Moufdi Hadjab, A study of CdTe solar cells using Ga-doped Mg$_x$Zn$_{1-x}$O buffer/TCO layers: Simulation and performance analysis, J. Sci.: Adv. Mater. Devices **4,** 111 (2019).

[42] K. Sasaki, A. Kuramata, T. Masui, E. G. Villora, K. Shimamura, and S. Yamakoshi, Device-quality β-Ga$_2$O$_3$ epitaxial films fabricated by ozone molecular beam epitaxy, Appl. Phys. Express **5,** 035502 (2012).

[43] S. W. Kaun, F. Wu, and J. S. Speck, β-(Al$_x$Ga$_{1-x}$)$_2$O$_3$/Ga$_2$O$_3$ (010) heterostructures grown on β-Ga$_2$O$_3$ (010) substrates by plasma-assisted molecular beam epitaxy, J. Vac. Sci. Technol. A **33,** 041508 (2015).

[44] F. K. Shan, G. X. Liu, W. J. Lee, G. H. Lee, I. S. Kim, and B. C. Shin, Structural, electrical, and optical properties of transparent gallium oxide thin films grown by plasma-enhanced atomic layer deposition, J. Appl. Phys. **98,** 023504 (2005).

[45] H. Altuntas, I. Donmez, C. Ozgit-Akgun, and N. Biyikli, Electrical characteristics of β-Ga$_2$O$_3$ thin films grown by PEALD, J. Alloys Compd. **593,** 190 (2014).

[46] H. C. Kang, Heteroepitaxial growth of multidomain Ga$_2$O$_3$/sapphire (001) thin films deposited using radio frequency magnetron sputtering, Mater. Lett. **119,** 123 (2014).

[47] H. Zhang, J. Deng, Z. Pan, Z. Bai, L. Kong, and J. Wang, Structural and optical properties of Nb-doped β-Ga$_2$O$_3$ thin films deposited by RF magnetron sputtering, Vacuum **146**, 93 (2017).

[48] S. J. Pearton, J. Yang, P. H. Cary, F. Ren, J. Kim, M. J. Tadjer, and M. A. Mastro, A review of Ga$_2$O$_3$ materials, processing, and devices, Appl, Phys. Rev. **5**, 011301 (2018).

[49] H. J. Bae, T. H. Yoo, Y. Yoon, I. G. Lee, J. P. Kim, B. J. Cho, and W. S. Hwang, High-Aspect ratio β-Ga$_2$O$_3$ nanorods via hydrothermal synthesis, Nanomaterials **8**, 594 (2018).

[50] C. G. Van De Walle and R. M. Martin, Theoretical study of band offsets at semiconductor interfaces, Phys. Rev. B **35**, 8154 (1987).

[51] A. Franciosi and C. G. Van De Walle, Heterojunction band offset engineering, Surf. Sci. Rep. **25**, 1 (1996).

[52] K. Steiner, W. Chen, and A. Pasquarello, Band offsets of lattice-matched semiconductor heterojunctions through hybrid functional and G$_0$W$_0$, Phys. Rev. B **89**, 205309 (2014).

[53] Y. Hinuma, A. Gruneis, G. Kresse, and F. Oba, Band alignment of semiconductors from density functional theory and many-body perturbation theory, Phys. Rev. B **90**, 155405 (2014).

[54] J. VandeVondele, M. Krack, F. Mohamed, M. Parrinello, T. Chassaing, and J. Hutter, QUICKSTEP: Fast and accurate density functional calculations using a mixed Gaussian and plane waves approach, Comput. Phys. Commun. **167**, 103 (2005).

[55] J. Hutter, M. Iannuzzi, F. Schiffmann, and J. VandeVondele, CP2K: Atomistic simulations of condensed matter systems, Wiley Interdiscip. Rev.: Comput. Mol. Sci. **4**, 15 (2014).

[56] J. VandeVondele and J. Hutter, Gaussian basis sets for accurate calculations on molecular systems in gas and condensed phases, J. Chem. Phys. **127**, 9 (2007).

[57] S. Goedecker, M. Teter, and J. Hutter, Separable dual-space Gaussian pseudopotentials, Phys. Rev. B **54**, 1703 (1996).

[58] See the Supplemental Material at http://link.aps.org/supplemental/10.1103/PhysRevApplied.15.034028 which includes references [69–82] for additional details about interface generation. The material's physical properties utilized for SCAPS simulations are also provided.

[59] M. Guidon, J. Hutter, and J. VandeVondele, Robust periodic hartree-fock exchange for large-scale simulations using gaussian basis sets, J. Chem. Theory Comput. **5**, 3010 (2009).

[60] M. Guidon, J. Hutter, and J. VandeVondele, Auxiliary density matrix methods for hartree-fock exchange calculations, J. Chem. Theory Comput. **6**, 2348 (2010).

[61] J. Schneider, J. Hamaekers, S. T. Chill, S. Smidstrup, J. Bulin, R. Thesen, A. Blom, and K. Stokbro, ATK-ForceField: A new generation molecular dynamics software package, Modelling Simul, Mater. Sci. Eng. **25**, 085007 (2017).

[62] D. Stradi, L. Jelver, S. Smidstrup, and K. Stokbro, Method for determining optimal supercell representation of interfaces, J. Phys. Condens. Matter **29**, 185901 (2017).

[63] S. Smidstrup, *et al.*, QuantumATK: An integrated platform of electronic and atomic-scale modelling tools, J. Phys.: Condens. Matter **32**, 015901 (2019).

[64] S. Mu, M. Wang, H. Peelaers, and C. G. Van de Walle, First-principles surface energies for monoclinic Ga$_2$O$_3$ and Al$_2$O$_3$ and consequences for cracking of (Al$_x$Ga$_{1-x}$)$_2$O$_3$, APL Mater. **8**, 091105 (2020).

[65] L. Weston, H. Tailor, K. Krishnaswamy, L. Bjaalie, and C. G. Van de Walle, Accurate and efficient band-offset calculations from density functional theory, Comput. Mater. Sci. **151**, 174 (2018).

[66] M. Burgelman, P. Nollet, and S. Degrave, Modelling polycrystalline semiconductor solar cells, Thin Solid Films **361**, 527 (2000).

[67] P. G. Mosesa and C. G. Van de Walle, Band bowing and band alignment in InGaN alloys, Appl. Phys. Lett. **96**, 021908 (2010).

[68] J. E. N. Swallow, R. G. Palgrave, P. A. E. Murgatroyd, A. Regoutz, M. Lorenz, A. Hassa, M. Grundmann, H. von Wenckstern, J. B. Varley, and T. D. Veal, Indium gallium oxide alloys: Electronic structure, optical gap, surface space charge, and chemical trends within common-cation semiconductors, ACS Appl. Mater. Interfaces **13**, 2807 (2021).

[69] J. Ahman, G. Svensson, and J. Albertsson, A reinvestigation of β-gallium oxide, Acta Crystallogr., Sect. C: Cryst. Struct. Commun. **52**, 1336 (1996).

[70] S. Geller, Crystal structure of β-Ga$_2$O$_3$, J. Chem. Phys. **33**, 676 (1960).

[71] F. Zhang, K. Saito, T. Tanaka, M. Nishio, and Q. Guo, Thermal annealing impact on crystal quality of (GaIn)$_2$O$_3$ alloys, J. Alloys Compd. **614**, 173 (2014).

[72] C. Kranert, J. Lenzner, M. Jenderka, M. Lorenz, H. von Wenckstern, R. Schmidt-Grund, and M. Grundmann, Lattice parameters and raman-active phonon modes of (In$_x$Ga$_{1-x}$)$_2$O$_3$ for $x < 0.4$, J. Appl. Phys. **116**, 013505 (2014).

[73] J. Heyd, J. E. Peralta, G. E. Scuseria, and R. L. Martin, Energy Band gaps and lattice parameters evaluated with the Heyd-Scuseria-Ernzerhof screened hybrid functional, J. Chem. Phys. **123**, 174101 (2005).

[74] O. Madelung, M. Schlz, and H. Weiss, *Numerical Data and Functional Relationships in Science and Technology, Landolt-Borstein* (Springer, Berlin, 1982), Vol. 17.

[75] H. He, R. Orlando, M. A. Blanco, R. Pandey, E. Amzallag, I. Baraille, and M. Rérat, First-principles study of the structural, electronic, and optical properties of Ga$_2$O$_3$ in its monoclinic and hexagonal phases, Phys. Rev. B **74**, 195123 (2006).

[76] M. Mohamed, C. Janowitz, I. Unger, R. Manzke, Z. Galazka, R. Uecker, R. Fornari, J. R. Weber, J. B. Varley, and C. G. Van de Walle, The electronic structure of β-Ga$_2$O$_3$, Appl. Phys. Lett. **97**, 211903 (2010).

[77] W. K. Metzger, S. Grover, D. Lu, E. Colegrove, J. Moseley, C. L. Perkins, X. Li, R. Mallick, W. Zhang, R. Malik, J. Kephart, C.-S. Jiang, D. Kuciauskas, D. S. Albin, M. M. Al-Jassim, G. Xiong, and M. Gloeckler, Exceeding 20% efficiency with in-situ group V doping in polycrystalline CdTe solar cells, Nat Energy **4**, 837 (2019).

[78] N. Romeo, A. Bosio, D. Menossi, A. Romeo, and M. Aramini, Last progress in CdTe/CdS thin film

solar cell fabrication process, Energy Procedia **57,** 65 (2014).

[79] S. Mu, H. Peelaers, Y. Zhang, M. Wang, and C. G. Van de Walle, Orientation-dependent band offsets between (Al$_x$Ga$_{1-x}$)$_2$O$_3$ and Ga$_2$O$_3$, Appl. Phys. Lett. **117,** 252104 (2020).

[80] M. Gloeckler, A. L. Fahrenbruch, and J. R. Sites, in *3rd World Conference on Photovoltaic Energy Conversion, Proceedings of Osaka*, 1, 491 (2003).

[81] Z. Zhang, E. Farzana, A. R. Arehart, and S. A. Ringel, Deep level defects throughout the bandgap of (010) β-Ga$_2$O$_3$ detected by optically and thermally stimulated defect spectroscopy, Appl. Phys. Lett. **108,** 052105 (2016).

[82] E. Farzana, M. F. Chaiken, T. E. Blue, A. R. Arehart, and S. A. Ringel, Impact of deep level defects induced by high energy neutron radiation in β-Ga$_2$O$_3$, APL Mater. **7,** 022502 (2019).